

Original paper

Horákite, a new hydrated bismuth uranyl–arsenate–phosphate mineral from Jáchymov (Czech Republic) with a unique uranyl-anion topology

Jakub PLÁŠIL^{1*}, Anthony R. KAMPF², Jiří SEJKORA³, Jiří ČEJKA³, Radek ŠKODA⁴, Jaromír TVRDÝ⁴

¹ Institute of Physics, Academy of Sciences of the Czech Republic (ASCR) v.v.i, Na Slovance 2, 182 21 Prague 8, Czech Republic; plasil@fzu.cz

² Mineral Sciences Department, Natural History Museum of Los Angeles County, 900 Exposition Boulevard, Los Angeles, CA 90007, USA

³ Department of Mineralogy and Petrology, National Museum, Cirkusová 1740, 193 00 Prague 9, Czech Republic

⁴ Department of Geological Sciences, Faculty of Science, Masaryk University, Kotlářská 2, 611 37 Brno, Czech Republic

* Corresponding author



Horákite, ideally $(\text{Bi}_7\text{O}_7\text{OH})[(\text{UO}_2)_4(\text{PO}_4)_2(\text{AsO}_4)_2(\text{OH})_2] \cdot 3.5\text{H}_2\text{O}$, is a new uranyl mineral discovered on a specimen originating from Jáchymov, Czech Republic (most probably from the Geister vein, Rovnost mine). It occurs as a supergene alteration mineral in association with phosphuranylite (overgrowing older metatorbernite–metazeunerite) in a quartz gangue with abundant tennantite. Horákite forms greenish-yellow to pale yellow prismatic crystals clustering to acicular aggregates, up to 1 mm across. Crystals are transparent to translucent with a vitreous luster. The mineral has a light yellow streak. Estimated Mohs' hardness is ~2. The cleavage is perfect on {100}. The calculated density is 6.358 g/cm³. Horákite is optically biaxial (+), $\alpha \approx 1.81$, $\beta \approx 1.84$, $\gamma \approx 1.88$ (measured in white light); $2V_{\text{obs}}$ is 78(1)°, $2V_{\text{calc}}$ is 83°; non-pleochroic. The optical orientation is $X = \mathbf{b}$, $Z \approx \mathbf{c}$. Electron-microprobe analysis yielded the empirical formula $(\text{Bi}_{7.01}\text{Pb}_{0.14})\text{O}_7\text{OH}[(\text{U}_{1.01}\text{O}_2)_4(\text{P}_{1.03}\text{O}_4)_2(\text{As}_{0.74}\text{Si}_{0.23}\text{O}_4)_2(\text{OH})_2] \cdot 3.5\text{H}_2\text{O}$ based on 37.5 O *apfu*. Horákite is monoclinic, $C2/c$, $a = 21.374(2)$, $b = 15.451(3)$, $c = 12.168(2)$ Å, $\beta = 122.26(1)^\circ$ and $V = 3398.1(10)$ Å³, $Z = 4$. The eight strongest X-ray powder-diffraction lines are [d_{obs} Å(I)(*hkl*)]: 11.77(100)(110), 6.21(23)(-202), 5.55(23)(310, -112), 4.19(27)(-331), 3.54(61)(510, -423), 3.29(20)(331), 3.14(58)(241, 023) and 3.02(98)(150, 113, -533, mult.). The crystal structure refinement of horákite, refined to $R = 5.95\%$ for 1774 unique observed reflections, revealed a novel sheet structure. It consists of topologically unique $[(\text{UO}_2)_4(\text{PO}_4)_2(\text{AsO}_4)_2(\text{OH})_2]$ sheets (*i.e.*, horákite topology), and an interstitial $\{(\text{Bi}_7\text{O}_7\text{OH})(\text{H}_2\text{O})_{3.5}\}$ complex. Sheets result from the polymerization of UO_7 bipyramids by sharing edges to form tetrameric units; tetrahedrally coordinated sites are linked to the UO_7 both monodentately ($T1$ to $U1$) and bidentately ($T2$ to $U2$). The mineral is named after František Horák (1882–1919), the mining engineer in Jáchymov, and his grandson, Vladimír Horák (born 1964), an amateur mineralogist and expert on the mining history of the Jáchymov ore district.

Keywords: horákite, new mineral, uranyl arsenate, crystal structure, topology, Jáchymov

Received: 7 February 2018; accepted: 20 August 2018; handling editor: F. Laufek

The online version of this article (doi: 10.3190/jgeosci. 267) contains supplementary electronic material.

1. Introduction

Uranyl phosphate and arsenate minerals are environmentally important phases that result from hydration–oxidation weathering of primary U minerals, mainly uraninite (Finch and Murakami 1999; Krivovichev and Plášil 2013; Plášil 2014). Generally, due to their low solubility products (see e.g., Ilton et al. 2010; Astilleros et al. 2013; Göb et al. 2013), they can occur both in the very leached parts of the uranium deposits (Finch and Murakami 1999; Plášil et al. 2006, 2009; Göb et al. 2013) and in mine dumps, wastes and tailings (Buck et al. 1995; Roh et al. 2000; Catalano et al. 2006; Cantrell et al. 2011; Maher et al. 2013). This makes uranyl phosphate and arsenate minerals essential in controlling U mobility in the environment. Currently,

there are approximately sixty valid uranyl phosphate and arsenate species. Herein, we report on the new mineral horákite, ideally $(\text{Bi}_7\text{O}_7\text{OH})[(\text{UO}_2)_4(\text{PO}_4)_2(\text{AsO}_4)_2(\text{OH})_2] \cdot 3.5\text{H}_2\text{O}$, which is the first uranyl mineral containing both phosphate and arsenate as essential components.

The new mineral honors two remarkable persons: mining engineer František Horák (1882–1919), who served from 1916 to 1918 as a formal chief of the Radium factory in St. Joachimsthal (Jáchymov), and his grandson, MUDr. (M.D.) Vladimír Horák (born 1964), who is an amateur mineral collector and historian, focused on the history of mining in Jáchymov. The new mineral was approved by the IMA Commission on New Minerals, Nomenclature and Classification (IMA 2017-033). The holotype specimen can be found in the mineralogical collection of the National

Museum in Prague (Czech Republic) under the catalog number PIP 17/2017. The crystals from the holotype used in this study are deposited in Natural History Museum of Los Angeles County (USA) under catalog number 66575.

2. Occurrence

Horákite was found on an old sample (probably discovered during first half of the 19th century) originating from Jáchymov (St. Joachimsthal), Czech Republic, preserved in a private collection of one of the authors (JT), and is now stored as a holotype. Despite the absence of the exact location, we can infer that sample comes from the Rovnost (formerly Werner) mine. Thorough details on the mineralogy, geology, and history of the Jáchymov ore district can be found elsewhere (Ondruš et al. 2003; Hloušek et al. 2014). The matrix of the fist-sized holotype sample is a (mylonitized) mica-schist containing thin quartz veinlets. The surface of the specimen exhibits abundant phosphuranylite overgrowing older metatorbernite–metazeunerite. Horákite occurs very sparingly in vugs of the quartz gangue. Primary minerals are represented by relics of tennantite and fine-grained uraninite. This association is typical of the Geister vein in the Rovnost mine (see, e.g. Plášil et al. 2017). The new mineral is of supergene origin, having formed *in-situ* in the oxidation zone. The inferred paragenetic sequence is metatorbernite/metazeunerite → phosphuranylite + horákite.

3. Physical and optical properties

Horákite occurs as prismatic to bladed crystals forming aggregates up to 1 mm across (Fig. 1). Crystals are



4. Chemical composition

The chemical composition of horákite was determined using a Cameca SX100 electron microprobe (WDS mode, 15 kV, 2 nA, and 5 μm beam diameter) at Masaryk University in Brno. Peak counting times were 10–20

Fig 1 Horákite crystal aggregate in a quartz gangue vug in association with blackish aggregates of tennantite (holotype specimen). Horizontal width of the picture is 2 mm, photo P. Škácha.

Tab. 1 Chemical composition of horákite from Jáchymov

Constituent	Mean of 21 spots (wt. %)	Range	SD	Standard
PbO	0.99	0.00–1.75	0.04	galena
Bi ₂ O ₃	50.22	49.00–51.33	0.63	metallic Bi
UO ₃	35.58	33.47–37.66	0.91	uranophane
SiO ₂	0.85	0.60–1.27	0.13	sanidine
P ₂ O ₅	4.47	4.09–5.91	0.41	fluorapatite
As ₂ O ₅	5.21	4.28–5.91	0.41	lammerite
H ₂ O*	2.77			
Total	100.09			

* H₂O content was calculated from stoichiometry (5 H₂O) derived from the crystal-structure study
SD – standard deviation

elongated on [001]. Crystals are transparent to translucent, greenish yellow to pale yellow and have a vitreous luster. The mineral has a light yellow streak and a Mohs' hardness of ~2. Prismatic crystals show at least one cleavage, perfect on {100}. A density of 6.358 g/cm³ was calculated using the empirical formula and unit-cell parameters obtained from single-crystal X-ray diffraction. Horákite is non-fluorescent under short- or long-wave UV radiation. The small size of the crystals and their high indices of refraction made the determination of the indices of refraction very difficult and only approximate values can be provided. Horákite is optically biaxial (+), with $\alpha \approx 1.81$, $\beta \approx 1.84$, $\gamma \approx 1.88$ (measured in white light). The $2V$ is 78(1)°, determined from extinction data using EXCALIBR (Gunter et al. 2004); the calculated $2V$ is 83°. Dispersion could not be observed. No pleochroism was observed. The optical orientation is $X = \mathbf{b}$, $Z \approx \mathbf{c}$. The Gladstone-Dale compatibility, $1 - (K_p/K_c)$, is -0.0568 (good) using the empirical formula, where $k(\text{UO}_3) = 0.118$, as provided by Mandarino (1976). As noted above, the measured indices of refraction are, at best, approximations.

s and the counting time for the background their half. The measured intensities were processed for matrix effects using the “PAP” correction routine (Pouchou and Pichoir 1985). The H₂O content (5 H₂O in total) was calculated by stoichiometry (obtained from the structure) on the basis of 37.5 O *apfu*. The analytical results are reported in Tab. 1. No other elements were detected; in particular, Al, Ca, Cl, F, Fe, K, Mg, Mn, Na and V, were sought and found to be below detection limits (~0.03–0.05 wt. % at the analytical conditions used).

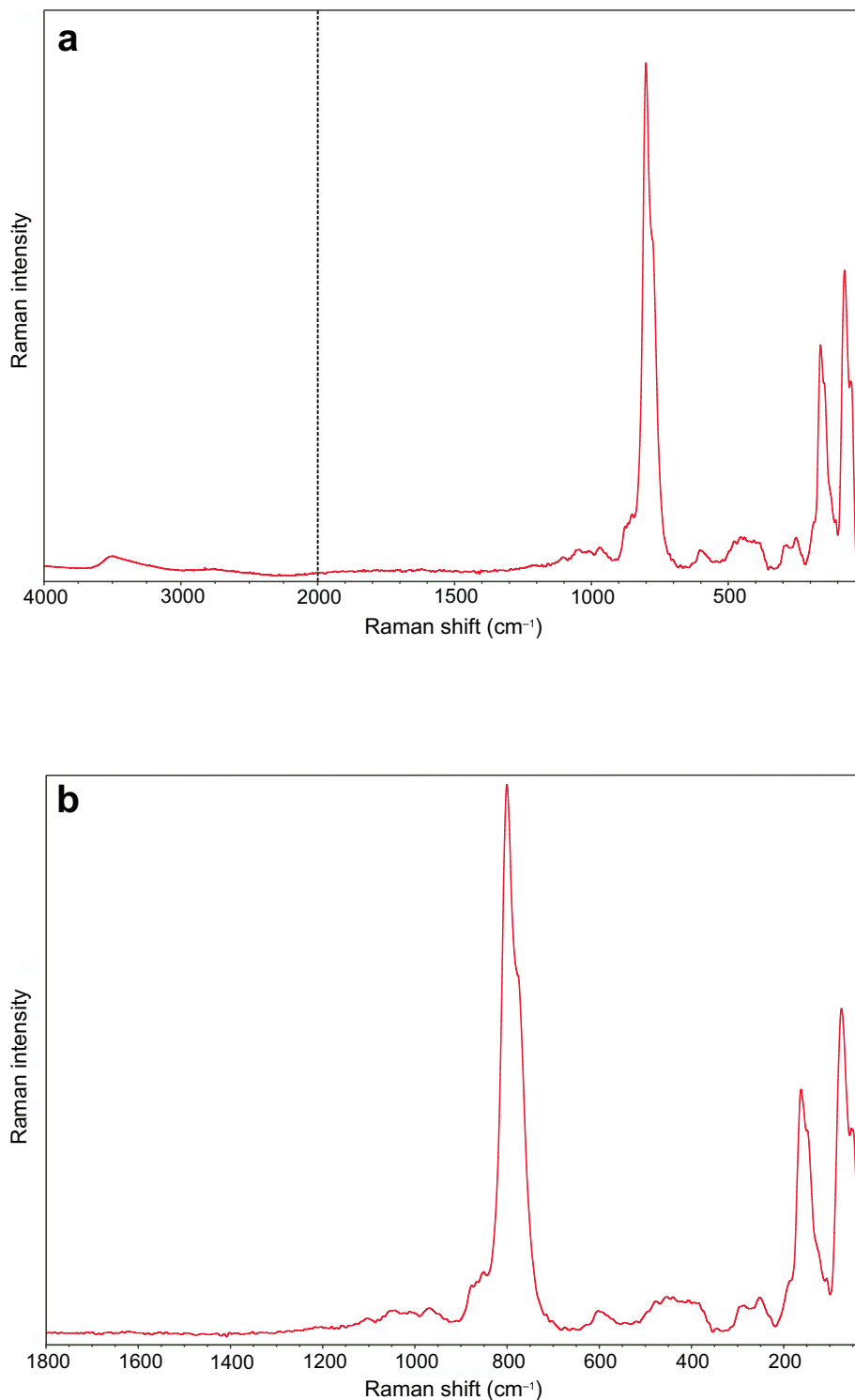
The empirical formula of horákité (calculated on the basis of 37.5 O *apfu*) is (Bi_{7.01}Pb_{0.14})O₇OH[(U_{1.01}O₂)₄(P_{1.03}O₄)₂(As_{0.74}Si_{0.23}O₄)₂(OH)₂]·3.5H₂O; this formula is well-balanced, showing 0.01 excess of a negative charge only. The ideal formula of horákité is (Bi₇O₇OH)[(UO₂)₄(PO₄)₂(AsO₄)₂(OH)₂]·3.5H₂O, which requires Bi₂O₃ 50.38, UO₃ 35.35, P₂O₅ 4.39, As₂O₅ 7.10 and H₂O 2.78, total 100 wt. %.

5. Raman spectroscopy

The Raman spectrum was collected in the range 4000–30 cm⁻¹ using a DXR dispersive Raman Spectrometer (Thermo Scientific) mounted on a confocal Olympus microscope. The Raman signal was excited by a green 532 nm diode-pumped solid-state laser and detected by a CCD detector. The experimental parameters were: 10× objective, 10 s exposure time, 100 exposures, 400 lines/mm grating, 25 μm pinhole spectrograph aperture and 0.4 mW laser power level. The instrument was set up by a software-controlled calibration procedure using multiple neon emission lines (wavelength calibration),

Fig. 2a – Raman spectrum of horákité in the range 4000–30 cm⁻¹ (split at 2000 cm⁻¹). **b** – Raman spectrum of horákité in the range 1800–30 cm⁻¹.

multiple polystyrene Raman bands (laser frequency calibration) and standardized white-light sources (intensity calibration). Spectral manipulations were performed using the Omnic 9 software (Thermo Scientific). Because of the complex structure of horákité (including P/As substitution and symmetrically non-equivalent U atoms), the coincidences and overlaps make any tentative attribu-



Tab. 2 Powder X-ray diffraction data for horákite (only calculated lines with $I_{\text{rel.}} > 1$ are listed)

$I_{\text{calc.}}$	$d_{\text{calc.}}$	h	k	l	$I_{\text{rel.}}$	d_{obs}
100	11.745	1	1	0	100	11.77
11	6.079	-2	0	2	23	6.21
13	5.613	3	1	0	23	5.55
12	5.460	-1	1	2		
13	4.949	-4	0	2	13	4.99
19	4.171	-3	3	1	27	4.19
13	3.863	0	4	0	15	3.87
11	3.702	2	0	2	17	3.69
10	3.616	0	4	1		
26	3.520	5	1	0	61	3.54
17	3.495	-4	2	3		
12	3.298	3	3	1	20	3.29
10	3.159	2	4	1	58	3.14
12	3.145	0	2	3		
16	3.046	1	5	0	98	3.02
13	3.022	1	1	3		
28	2.973	-5	3	3	35	2.92
14	2.918	-2	0	4		

d values quoted in Å

tion of observed bands to individual vibrations difficult. Observed lowering of symmetry of the structural units causes corresponding Raman activation of some or all

Tab. 3 Crystallographic data and refinement details for horákite

Structural formula	$(\text{Bi}_7\text{O}_7\text{OH})[(\text{UO}_2)_4(\text{PO}_4)_{2.741}(\text{AsO}_4)_{1.259}(\text{OH})_2] \cdot 3.5\text{H}_2\text{O}$
a, b, c [Å]	21.374(2), 15.451(3), 12.168(2)
β [°]	122.261(13)
V [Å ³]	3398.1(10)
Z	4
D_{calc} [g/cm ³]	6.263
Space group	$C2/m$
Temperature	297 K
Diffraction; wavelength	Rigaku SuperNova with Atlas S2 CCD detector
X-ray radiation/power	MoK_α (0.71073 Å)/50 kV, 40 mA
Crystal dimensions [mm]	0.020 × 0.012 × 0.010
Collection mode	ω rotational scans
Limiting θ angles [°]	3.70–26.81°
Limiting Miller indices	$-22 < h < 26, -15 < k < 21, -14 < l < 16$
No. of reflections	8703
No. of unique reflections	3574
No. of observed reflections (criterion)	1744 [$I_{\text{obs}} > 3\sigma(I)$]
R_{int}	0.128
Absorption correction (mm ⁻¹), method	56.56, Gaussian (Jana2006)
Transmission (min/max)	0.4429/0.6699
F_{000}	5325
Refinement by Jana2006 on F^2	
Parameters refined, constraints, restraints	152, 0, 21
R, wR (obs)	0.0595, 0.1131
R, wR (all)	0.1350, 0.1458
GOF obs/all	1.22/1.09
$\Delta\rho_{\text{min}}, \Delta\rho_{\text{max}}$ (eÅ ⁻³)	-6.08, 11.51 (0.11 Å to Bi3)
Weighting scheme, details	$\sigma, w = 1/(\sigma^2(I) + 0.0004I^2)$

vibrations and splitting of doubly- or triply-degenerate ones. The Raman spectrum was interpreted with reference to Nakamoto (1986), Čejka (1999), Sejkora et al. (2002, 2004, 2008), Ardelean et al. (2006) and Frost et al. (2011) and references therein.

The full-range Raman spectrum of horákite is shown in Fig. 2a. An observed weak broad-band at 3580 cm⁻¹ with a shoulder at 3410 cm⁻¹ is connected with the ν O–H stretching vibrations of hydrogen-bonded OH⁻ and H₂O molecules. Approximate O–H...O hydrogen bond lengths vary in the range from 3.2 to 2.81 Å (Libowitzky 1999).

The spectrum in the range 1800–30 cm⁻¹ is shown in Fig. 2b. No Raman band was observed in the region where the ν_2 (δ) H–O–H bending vibrations should occur. A series of weak bands between 1200 and 1030 cm⁻¹ (1103, 1081, 1069, 1055 and 1039 cm⁻¹) may be attributed to the triply degenerate ν_3 antisymmetric stretching vibration of (PO₄)³⁻ polyhedra; those between 1030 and 930 cm⁻¹ to the ν_1 symmetric stretching vibration of (PO₄)³⁻ polyhedra.

The ν_3 (UO₂)²⁺ vibrations, activated in the Raman spectrum by symmetry distortion, may be connected with the bands at 879 and 864 cm⁻¹, while the ν_1 (UO₂)²⁺ symmetric stretching vibration is present as a very strong band centered at 801 cm⁻¹ with a shoulder at 850 cm⁻¹. Bartlett and Cooney (1989) provided an empirical formula to derive the approximate U–O bond lengths from the band positions assigned to the (UO₂)²⁺ stretching vibrations (Å/cm⁻¹): 1.80/879, 1.81/866, 1.76/850, 1.81/801. These values are in accordance with U–O bond lengths given in general by Burns et al. (1997) and Lussier et al. (2016) for the U–O bond-length in UO₇ polyhedra and from the current crystal-structure data. A coincidence of the ν_1 (UO₂)²⁺ stretching, the δ -UOH (in-plane) bending modes and the triply degenerate ν_3 antisymmetric stretching vibration of (AsO₄) tetrahedra in this region is assumed.

The band at 774 cm⁻¹ is assigned to the ν_1 symmetric stretching vibration of (AsO₄). A series of weak bands observed in the 640–520 cm⁻¹ region may be attributed to the triply degenerate ν_4 bending vibrations of (PO₄) tetrahedra and Bi–O stretching vibrations. The complex composite band between 510 and 360 cm⁻¹ is

probably connected with the doubly degenerate ν_2 bending vibrations of (PO_4) , the triply degenerate ν_3 bending vibrations of (AsO_4) , Bi–O stretching and Bi–O–Bi bending vibrations. The bands at between 380 and 280 cm^{-1} may be assigned to the doubly degenerate ν_2 bending vibrations of (AsO_4) and Bi–O stretching vibrations. According to Ardelean et al. (2006), bands close to $\sim 235 \text{ cm}^{-1}$ may be assigned to the Bi–O bonds vibrations in BiO_3 and BiO_6 polyhedra, bands close to $\sim 315 \text{ cm}^{-1}$ to Bi–O–Bi stretching vibrations in distorted BiO_6 polyhedra, and bands close to $\sim 585 \text{ cm}^{-1}$ to the Bi–O stretching vibrations in BiO_6 polyhedra. The band at 251 cm^{-1} with shoulders at 271 and 228 cm^{-1} is connected with the doubly degenerate ν_2 bending vibrations of $(\text{UO}_2)^{2+}$ groups. The remaining bands $< 200 \text{ cm}^{-1}$ (189, 163, 147, 123, 105, 74 and 48 cm^{-1}) are assigned to external lattice vibration modes and $(\text{UO}_2)^{2+}$ translations and rotations.

6. X-ray crystallography and crystal structure

The X-ray powder-diffraction data for horákite (Tab. 2) were recorded using a Rigaku R-Axis Rapid II curved imaging plate microdiffractometer with monochromated MoK_α radiation. A Gandolfi-like motion on the φ and ω axes was used to randomize the sample. Theoretical diffraction powder pattern was calculated by PowderCell program (Kraus and Nolze 1996) from crystal-structure data. Due to a low quality of the powder-diffraction pattern and a low symmetry of horákite structure only comparison between calculated and observed d -spacing and intensities is given.

A $0.020 \times 0.012 \times 0.010 \text{ mm}$ prismatic crystal of horákite was selected for single-crystal X-ray diffraction experiment using a Rigaku SuperNova single-crystal four-circle diffractometer with kappa-geometry and mirror-monochromatized MoK_α radiation ($\lambda = 0.71073 \text{ \AA}$) from a micro-focus X-ray tube. Diffracted X-rays were recorded with an Atlas S2 CCD detector. Horákite is monoclinic, with space group $C2/c$, and cell parameters: $a = 21.374(2)$, $b = 15.451(3)$, $c = 12.168(2) \text{ \AA}$, $\beta = 122.26(1)^\circ$ and $V = 3398.1(10) \text{ \AA}^3$, $Z = 4$. The summary of experimental conditions, crystallographic data and refinement results is listed in Tab. 3.

Tab. 4 Atom positions and displacement parameters (in \AA^2) in the structure of horákite

Atom	Occupancy	x/a	y/b	z/c	U_{eq}
Bi1		0.55568(7)	0.59587(8)	0.52965(11)	0.0138(5)
Bi2		0.5	0.77560(12)	0.25	0.0143(8)
U1		0.80049(7)	0.57582(8)	0.64664(11)	0.0135(5)
Bi3		0.37269(7)	0.60815(9)	0.23420(12)	0.0183(6)
Bi4		0.41117(7)	0.39403(9)	0.11847(12)	0.0196(6)
U2		0.69234(8)	0.82367(9)	0.83708(13)	0.0225(6)
As1/P1	0.57(2)/0.43(2)	0.6842(2)	0.7689(3)	0.5517(4)	0.011(2)
P2/As2	0.94(2)/0.06(2)	0.7521(4)	0.5905(5)	0.8885(7)	0.013(4)
O1		0.4750(11)	0.6828(13)	0.3449(18)	0.011(2)*
O2		0.6774(12)	0.5491(15)	0.803(2)	0.023(6)*
O3		0.4392(11)	0.5459(13)	0.4273(18)	0.011(2)*
O4		0.4726(11)	0.3751(13)	0.3278(18)	0.011(2)*
O5		0.7813(14)	0.8500(17)	0.857(2)	0.034(7)*
O6		0.7620(13)	0.7165(15)	0.621(2)	0.020(6)*
O7		0.7970(14)	0.5993(17)	0.826(2)	0.031(6)*
O8		0.6060(15)	0.7903(18)	0.824(2)	0.041(8)*
O9		0.7389(12)	0.6873(15)	0.924(2)	0.020(6)*
O10		0.6216(12)	0.7231(14)	0.4113(19)	0.014(5)*
O11		0.6511(12)	0.7619(14)	0.6426(19)	0.016(5)*
O12		0.8938(12)	0.6088(14)	0.733(2)	0.019(5)*
O13		0.7031(13)	0.9524(16)	0.976(2)	0.023(6)*
O14		0.4327(11)	0.5307(13)	0.1590(18)	0.011(2)*
O15		0.7048(12)	0.5478(14)	0.5613(19)	0.017(5)*
O16		0.6985(13)	0.8696(15)	0.533(2)	0.021(6)*
O17		0.6489(15)	0.9442(19)	0.725(2)	0.043(8)*
O18	0.5	0.909(3)	0.729(4)	0.975(5)	0.044(15)*
O19	0.5	0.528(4)	0.868(5)	0.463(6)	0.08(2)*
O20	0.5	0.596(4)	0.973(4)	0.508(6)	0.059(19)*
O21	0.25	0.503(7)	0.931(8)	0.687(10)	0.05(3)*

U_{eq} is defined as a third of the trace of the orthogonalized U^{ij} tensor

* – refined with isotropic displacement parameters

The structure of horákite was solved from the single-crystal X-ray data using the SHELXT program (Sheldrick 2015) and refined by the full-matrix least-squares algorithm of the Jana2006 software (Petříček et al. 2014) based on F^2 . The initial structure solution suggested unambiguously a C -centered cell and the centrosymmetric space group $C2/c$, which was confirmed by the subsequent refinement. Several atoms missing in the initial structure model (e.g., O18, O19, O20, O21) were found from the difference Fourier maps. Two tetrahedrally coordinated sites were refined with joint occupancies by P and As. Only for U, Bi and P/As sites the anisotropic atomic displacement parameters were used; in case of O atoms isotropic displacement parameters were used instead. A final difference Fourier map failed to indicate possible locations of H atoms, which is not unusual for a U compound; moreover, here it is due to weak data. The refinement for 151 parameters converged smoothly to a final $R = 0.0573$, $wR = 0.1017$ for 1743 observed reflections with goodness of fit (GOF) of 1.16. Refinement results are given in Tab. 3, atomic coordinates and displacement parameters in Tab. 4, anisotropic displacement parameters in the Electronic

Tab. 5 Selected interatomic distances (in Å) in the crystal structure of horákite

U1–O6	2.29(2)	U2–O5	1.83(3)		
U1–O7	2.25(3)	U2–O8	1.84(3)		
U1–O12	1.76(2)	U2–O9	2.33(2)		
U1–O13 ^v	2.39(3)	U2–O9 ^{vii}	2.46(2)		
U1–O15	1.78(2)	U2–O11	2.25(2)		
U1–O16 ⁱⁱⁱ	2.35(3)	U2–O13	2.54(3)		
U1–O17 ^v	2.44(3)	U2–O17	2.20(3)		
<U1–O _{ur} >	1.77	<U2–O _{ur} >	1.83		
<U1–O _{eq} >	2.34	<U2–O _{eq} >	2.36		
<i>T1</i> –O6	1.62(2)	<i>T2</i> –O2	1.51(2)		
<i>T1</i> –O10	1.664(18)	<i>T2</i> –O7	1.52(4)		
<i>T1</i> –O11	1.60(3)	<i>T2</i> –O9	1.62(2)		
<i>T1</i> –O16	1.63(2)	<i>T2</i> –O13 ^{vii}	1.55(2)		
< <i>T1</i> –O>	1.63	< <i>T2</i> –O>	1.55		
Bi1–O1	2.385(18)	Bi2–O1	2.08(2)	Bi3–O1	2.186(19)
Bi1–O2	3.016(19)	Bi2–O1 ⁱⁱ	2.08(2)	Bi3–O2 ⁱ	2.60(2)
Bi1–O3	2.24(2)	Bi2–O10	2.413(19)	Bi3–O3	2.213(18)
Bi1–O3 ⁱ	2.24(2)	Bi2–O10 ⁱⁱ	2.413(19)	Bi3–O5	3.10(4)
Bi1–O4 ⁱ	2.17(3)	Bi2–O12 ⁱⁱⁱ	2.81(3)	Bi3–O10 ⁱⁱ	2.56(2)
Bi1–O14 ⁱⁱ	2.64(3)	Bi2–O12 ^{iv}	2.81(3)	Bi3–O14	2.27(3)
Bi1–O15	3.09(3)	Bi2–O19	2.74(9)	<Bi3–O>	2.49
<Bi1–O>	2.54	Bi2–O19 ⁱⁱ	2.74(9)		
		<Bi2–O>	2.51		
		Bi4–O2 ⁱ	2.69(3)		
		Bi4–O3 ^{vi}	2.85(3)		
		Bi4–O4	2.174(19)		
		Bi4–O4 ⁱⁱ	2.22(2)		
		Bi4–O5	2.97(2)		
		Bi4–O8	3.00(3)		
		Bi4–O14	2.16(2)		
		Bi4–O18	3.07(6)		
		<Bi4–O>	2.64		

Symmetry codes: (i) $-x+1, -y+1, -z+1$; (ii) $-x+1, y, -z+1/2$; (iii) $-x+3/2, -y+3/2, -z+1$; (iv) $x-1/2, -y+3/2, z-1/2$; (v) $-x+3/2, y-1/2, -z+3/2$; (vi) $x, -y+1, z-1/2$; (vii) $-x+3/2, -y+3/2, -z+2$; (viii) $x+1/2, -y+3/2, z+1/2$; (ix) $-x+3/2, y+1/2, -z+3/2$; (x) $x, -y+2, z+1/2$; (xi) $-x+1, -y+2, -z+1$

Supplementary Material (Tab. S1), selected interatomic distances in Tab. 5, and results of bond-valence analysis in Tab. 6. The bond-valence analysis was carried out following the procedure of Brown (2002). The CIF file, also containing a block with the reflections, is deposited at the Journal's web page www.jgeosci.org.

6.1. Crystal structure

The asymmetric unit of horákite (Fig. 3) contains two U sites, four Bi sites, two *T* sites jointly occupied by P and As, and twenty O sites (of which three belong to OH and four to H₂O; Tab. 6). Each U site is coordinated by seven ligands, forming pentagonal bipyramids, whereby the apices of each bipyramid are comprised of strongly bonded (~1.8 Å) O atoms, forming the approximately lin-

ear uranyl ion – UO₂²⁺ (Tab. 5). In the equatorial plane, each uranyl ion is linked to five ligands, either O or OH (O17 atom). Uranyl polyhedra polymerize by sharing equatorial edges to form tetrameric units; tetrahedrally coordinated sites are linked to the UO₇ bipyramids in two distinct ways, as monodentate (*T1* to U1) or bidentate (*T2* to U2) linkages (Fig. 4). The *T1* site was found to be dominantly occupied by As⁵⁺. The *T2* site is nearly fully occupied by P⁵⁺ (94 %). Through *T1* tetrahedra, adjacent four-membered clusters are linked along [010]. These chains are then linked *via* *T*–O bonds to adjacent chains to form corrugated sheets parallel to {100} (Fig. 5). Between these sheets, there is a (Bi₇O₇OH)⁶⁻ complex, which involves one [6]-coordinated, one [7]-coordinated and two [8]-coordinated Bi³⁺ cations (Tab. 5) and H₂O groups linked by H-bonds to the sheets, as well as to the Bi-complex. The Bi–O bonds link Bi atoms into a 3D chain structure, which extends parallel to *c* (Fig. 3). There are a few O atoms within the interstitial complex (bonded to Bi) that have a low *U*_{eq} value. The low *U*_{eq} either suggests a possible presence of a heavier anion at the sites, maybe F⁻ (however,

no F was indicated in the WDS analysis), or it is just an artifact due to poorly fitted absorption effects.

Therefore, we assume from the refinement the structural formula for horákite to be (Bi₇O₇OH)[(UO₂)₄(PO₄)_{2,7}₄₁(AsO₄)_{1,259}(OH)₂]₃·3.5H₂O, *Z* = 4, which is electroneutral. However, the exact mechanism of the charge balance in the interlayer remains unclear because of the limited quality of the X-ray data.

6.2. Structural and chemical complexity

The structural complexity of horákite and related minerals was determined as the Shannon information content per atom (*I*_G) and per unit cell (*I*_{G,total}). The concept of Shannon information, also known as Shannon entropy, used herein originates from information theory. This

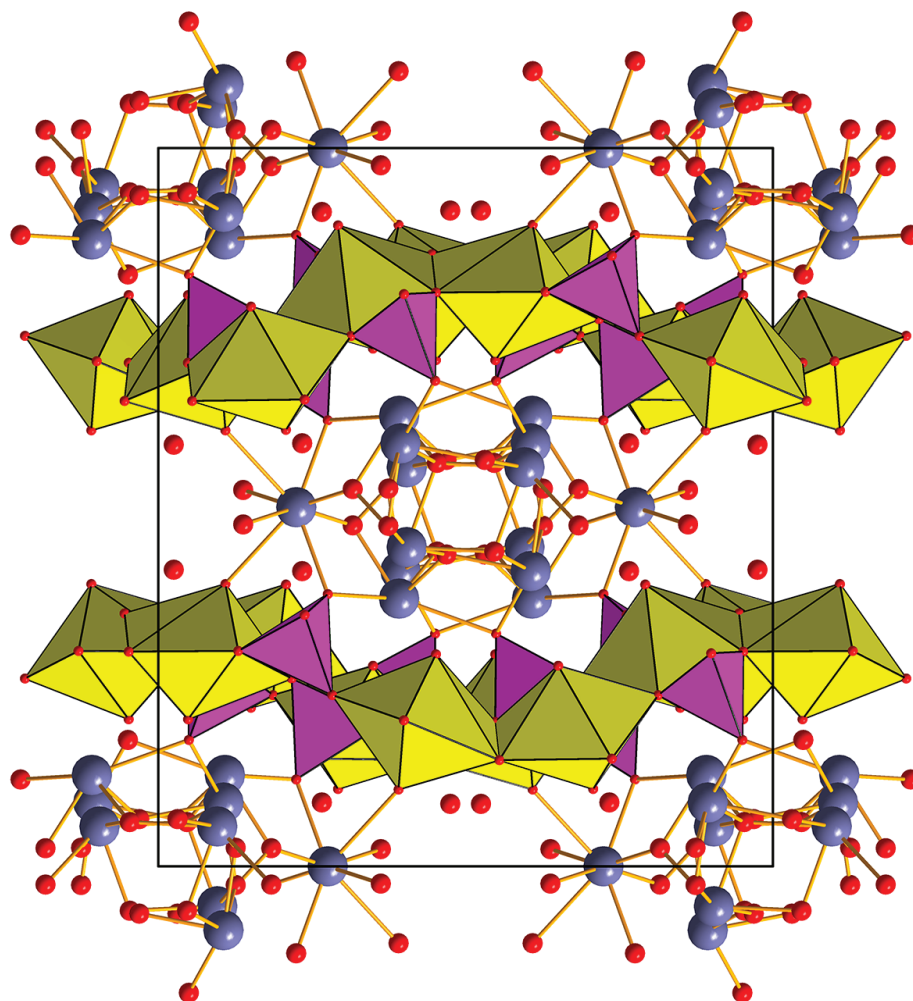


Fig. 3 Polyhedral representation of the horákité structure viewed down to *c* axis (UO_7 = yellow, TO_4 = violet, Bi = blue, interstitial O = red). Unit-cell edges are outlined by black solid lines.

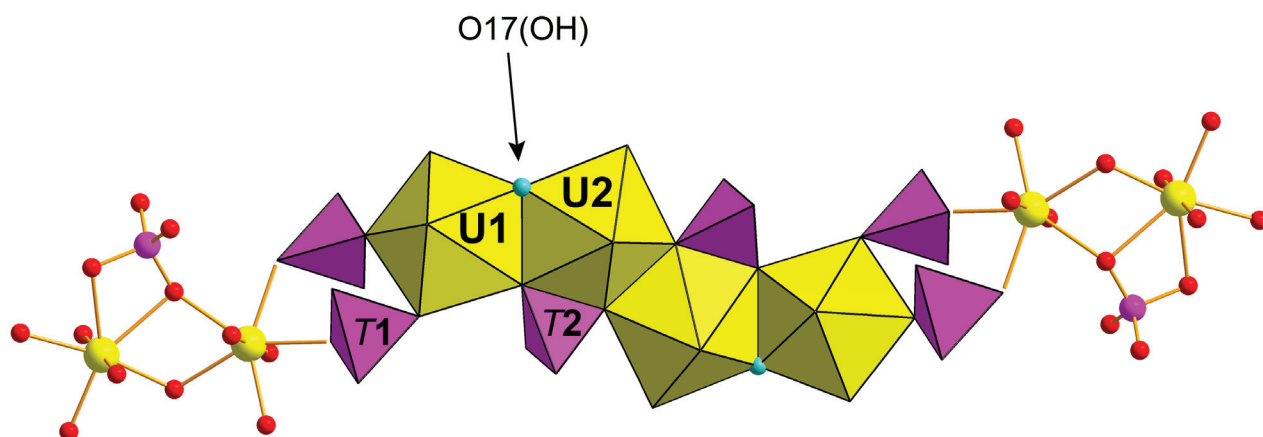


Fig. 4 Fundamental building block of the uranyl phosphate sheet found in horákité: a tetramer of the edge-sharing UO_7 bipyramids (yellow) with two bidentate symmetrically related T_2 tetrahedra and four symmetrically related T_1 tetrahedra that link adjacent tetramers (ball-and-stick model) into infinite chains along *b*. The O17 site (OH) is shown as a blue sphere.

approach was developed by Krivovichev (2012, 2013, 2014, 2016, 2017): the complexity of a crystal structure can be quantitatively characterized by the amount of

Shannon information, which is measured in bits (binary digits) per atom (bits/atom) and per unit cell (bits/cell), respectively. The amount of Shannon information

Tab. 6 Bond-valence analysis of the horákite structure

	U1	U2	Bi1	Bi2	Bi3	Bi4	T1*	T2	Σ BV	Assignment
O1			0.44	0.97×2↓	0.74				2.15	O
O2			0.09		0.25	0.20		1.33	1.87	O+H
O3			0.65×2↓		0.69	0.13			1.47	OH*
O4			0.77			0.76;0.68			1.49	OH*
O5		1.52			0.07	0.10			1.69	O+H
O6	0.62						1.30		1.91	O
O7	0.67							1.30	1.97	O
O8		1.49				0.09			1.59	O+H
O9		0.57;0.44						1.01	2.03	O
O10				0.41×2↓	0.28		1.15		1.85	O+H
O11		0.67					1.37		2.04	O
O12	1.75			0.15×2↓					1.90	O
O13	0.51	0.38						1.20	2.09	O
O14			0.23		0.59	0.79			1.61	O+H
O15	1.68		0.07						1.75	O+H
O16	0.55						1.26		1.81	O+H
O17	0.46	0.74							1.20	OH
O18						0.08			0.08	H ₂ O
O19				0.36×2↓					0.36	H ₂ O
O20									0.00	H ₂ O
O21									0.00	H ₂ O
Σ BV	6.24	5.82	2.89	3.42	2.63	2.83	5.07	4.84		

Values are given in valence units (*vu*)

Σ BV = sum of bond-valences incident at the atomic site; OH* – the site has partially OH character; O+H – there is a least one H-bond (~0.2 *vu*) accepted by the anion

The bond valence parameters for U⁶⁺–O taken from Burns et al. (1997), other bond-valence parameters from Gagné and Hawthorne (2015)

T1* – site considered as mixed site with occupancies 0.57 As, and 0.43 P

reflects the diversity and relative proportion of different objects, *e.g.*, the number and relative proportion of different sites in an elementary unit cell of a crystal structure.

The information-based structural-complexity values were calculated using the software package TOPOS (Blatov et al. 2014). The chemical complexity (after Siidra et al. 2014) was estimated by considering chemical formula as a message, where symbols correspond to different chemical elements. Structural and chemical complexity values are given in Tab. 7.

the sheet (Figs 4 and 5). Thus, orientational stereoisomerism can occur (Krivovichev 2009, 2010). In the sheet anion topology of horákite, we can discern tetrahedra (T1 and T2, respectively) related to empty squares and tetrahedra related to distorted pentagons (*i.e.*, bidentately linked tetrahedra) (Fig. 5). The empty squares between T1 and T2 positions connect one *down*, and one *up* tetrahedron. There are also empty diamonds/rhomboids connecting two T1 sites, one oriented *up* and one oriented *down*. There are also distorted pentagons that connect one *up*, and one *down*, T1 and T2 tetrahedra (Fig. 5).

7. Discussion

7.1. The topology of the uranyl-anion sheets

Horákite, due to above-mentioned substitution, is the P-dominated member of the assumed series, containing, however, significant amount of As. We can only speculate about an ideal composition of the P-dominated end-member sheet, which can be [(UO₂)₄(PO₄)₄(OH)₂]⁶⁻, and of the As-dominated end-member sheet that can be [(UO₂)₄(AsO₄)₄(OH)₂]⁶⁻. It is a topologically unique sheet among known uranyl minerals and synthetic compounds. The graphical representation of the sheet anion topology, which consists of pentagons, squares, and triangles, is displayed in Fig. 6. Both tetrahedra are connected to three U polyhedra with the fourth vertex of each tetrahedron non-linked within

Tab. 7 The complexity measures for horákite and related minerals (calculations include H atoms)

Mineral	Chemical formula	Spgr.	V (Å ³)	ν	I_G (bits/atom)	$I_{G, total}$ (bits/cell)	I_{chem} (bits/formula)	Reference
Hügelite	Pb ₂ [(UO ₂) ₃ O ₂ (AsO ₄) ₂](H ₂ O) ₅	$P2_1/m$	3762	304	6.41	1947.37	65.21	1)
Phosphuranylite	K ₂ Ca[(UO ₂) ₇ (PO ₄) ₄ O ₂ (OH) ₂](H ₂ O) ₈ *	$Cmcm$	3765	152	5.04	765.69	128.31	2)
Horákite	(Bi ₇ O ₇ OH)[(UO ₂) ₄ (PO ₄) _{2.74} (AsO ₄) _{1.26} (OH) ₂]·3.5H ₂ O	$C2/c$	3398	134	5.11	684.86	111.91	3)
Kamitugaite	PbAl[(UO ₂) ₂ (PO ₄) _{2.38} (AsO ₄) _{0.62} O ₂ (OH) ₂](H ₂ O) _{11.5}	$P-1$	1553	96	5.59	536.16	131.58	4)
Dumontite	Pb ₂ [(UO ₂) ₃ O ₂ (PO ₄) ₂](H ₂ O) ₅	$P2_1/m$	903	76	4.41	334.84	65.21	5)
Hallimondite	Pb ₂ [(UO ₂)(AsO ₄) ₂](H ₂ O) _{0.5}	$P-1$	499	32	4.00	128.00	27.11	6)
Walpurgite	(BiO) ₄ (UO ₂)(AsO ₄) ₂ (H ₂ O) ₂	$P-1$	374	25	3.68	92.10	54.87	7)

Spgr. – space group; * – the electroneutral formula proposed for phosphuranylite, derived from new structure determinations (unpublished data of authors). References: 1) Locock and Burns (2003), 2) Demartin et al. (1991), 3) this paper, 4) Plášil (2017), 5) Piret and Piret-Meunier (1988), 6) Locock et al. (2005), 7) Mereiter (1982)

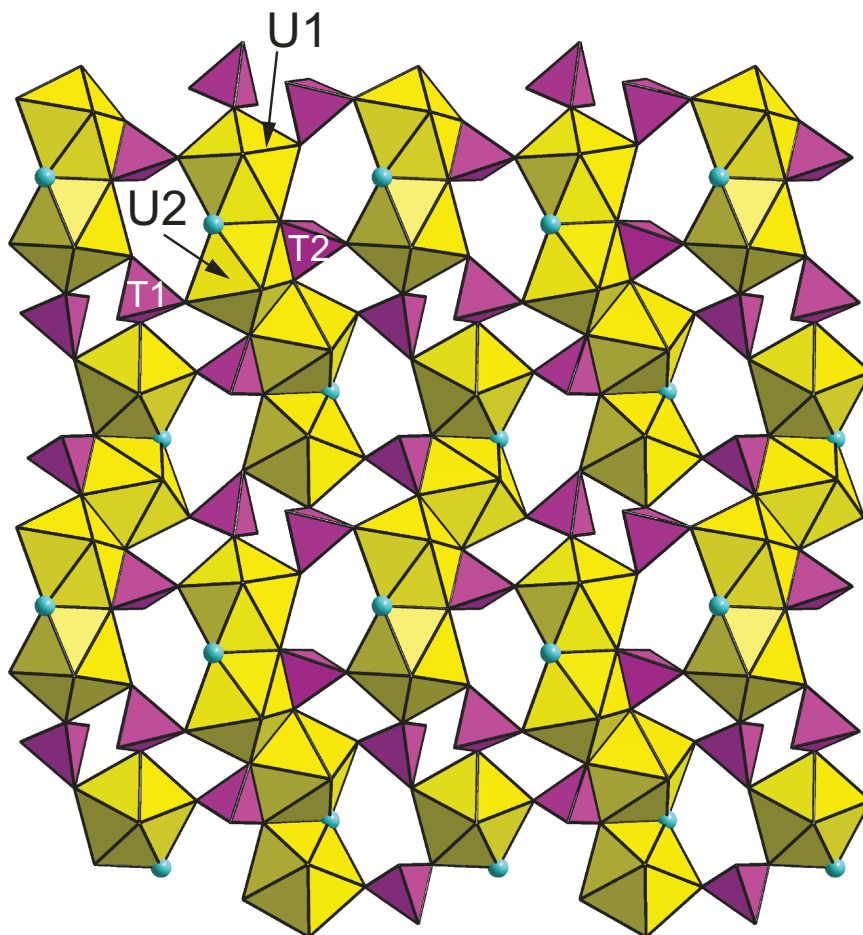


Fig. 5 Uranyl phosphate sheet found in the structure of horákite; the O17 site (OH) is shown as a blue sphere.

These empty diamonds/rhomboids are a rather unique topological feature in the crystal chemistry of U^{6+} compounds. Somewhat similar are distorted diamonds in sheets of the synthetic phases $K[(UO_2)(CrO_4)(OH)] \cdot 1.5H_2O$ (Serezhkina et al. 1990), $Cs[(UO_2)(OH)(SeO_4)] \cdot H_2O$ (Serezhkina et al. 2010) or $Cs[(UO_2)F(PO_3OH)] \cdot 0.5H_2O$ (Ok et al. 2006).

7.2. The presence of As^{5+} in the structure of horákite

It is highly interesting that in the horákite structure one of the tetrahedral sites (As1/P1) was found to be slightly dominated by As^{5+} over P^{5+} , while the second site (P2/As2) far more by P^{5+} . It seems to be reasonable that larger As^{5+} (ionic radius of 0.34 Å; Shannon 1976) is entering monodentately linked T1 tetrahedron, while bidentately linked T2 tetrahedron is occupied by much smaller P^{5+} (0.17 Å; Shannon 1976). The repulsion in case of As^{5+} would probably destabilize the structure. We can only speculate whether the As is essential for the stability of horákite. Nevertheless, horákite growth is probably a consequence of formation in the P-rich environment,

where, however, still some As^{5+} is present (from oxidation of tennantite). Somewhat similar circumstances were observed in case of the uranyl phosphate–arsenate mineral kamitugaite (Plášil 2017).

7.3. The status of horákite and the related minerals

As stated above, horákite represents a possible ordered intermediate member between two yet unknown end-members. Their respective theoretical formulae are $(Bi_7O_7OH)[(UO_2)_4(PO_4)_4(OH)_2] \cdot 3.5H_2O$ and $(Bi_7O_7OH)[(UO_2)_4(AsO_4)_4(OH)_2] \cdot 3.5H_2O$. It should be mentioned that the U : T (T = As and/or P) ratio (4 : 4 or their factors) of the uranyl-anion sheet in horákite is similar to that in autunite-group minerals (1 : 1; Locock 2007). Nevertheless, the *metal(Me)* : U : T is distinctive; for horákite it is 7 : 4 : 4 and for autunite-group minerals, e.g. for arsenuranospathite (Dal Bo et al. 2015), it is 1 : 2 : 2.

Horákite is a new member of Strunz class 08.ED; unclassified uranyl phosphates and arsenates. Visually, it most resembles parsonsite, hügelite and walpurgite; however; these three minerals have completely distinct

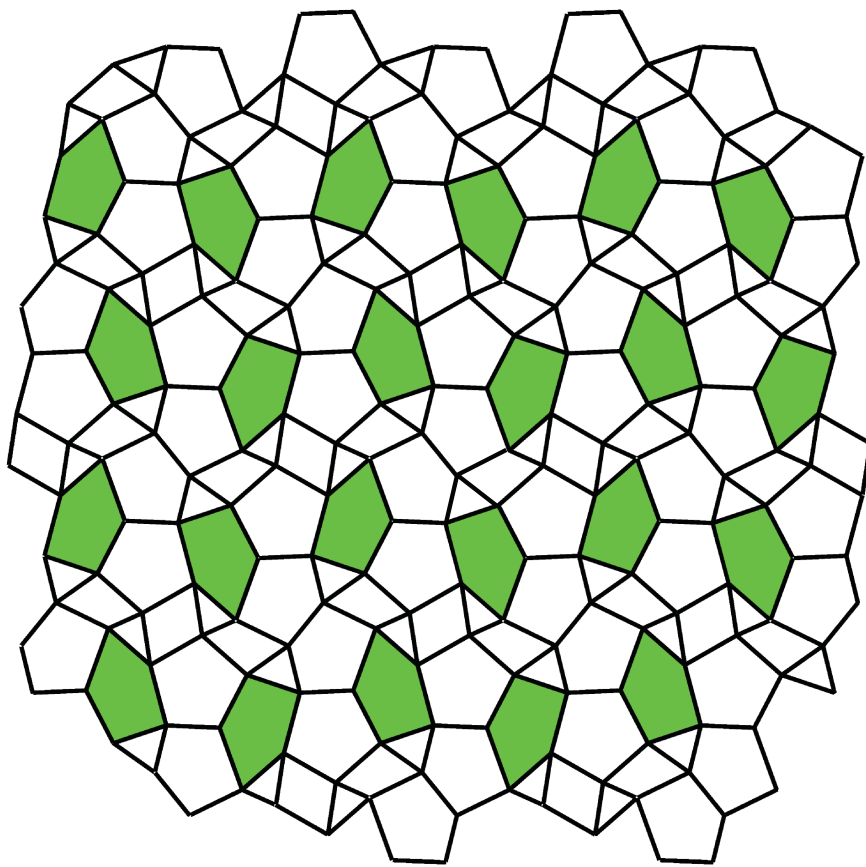


Fig. 6 Graphical representation of horákite uranyl anion topology, which consists of pentagons, squares and triangles. The large irregular green pentagons, as well as the squares, are not occupied in horákite.

structures (containing clusters of chains of U^{6+} polyhedra). The Bi uranyl–arsenate walpurgite has a higher Bi:U proportion (4:1) than horákite (7:4).

7.4. Structural and chemical complexity and remarks on horákite origin

Horákite and related uranyl phosphates and arsenates are listed in Tab. 7 along with their structural and chemical complexities. Horákite, with 685 bits/cell, qualifies as a complex mineral in the classification scheme of Krivovichev (2013). It is similar in complexity to phosphuranylite (766 bits/cell), which was found in the direct association with horákite, and kamitugaite (536 bits/cell), which has a complicated sheet similar to that in phosphuranylite. Their high chemical complexities (>100 bits/fu; see Plášil 2018) may relate to the fact that they are all late-stage alteration phases with rather high *Me* proportions or the presence of multiple chemical elements (derived during the weathering process).

Unambiguously, the most common Bi–U–O–H mineral not only in Jáchymov, but in general, is walpurgite, a simple phase both structurally and chemically. Hügelite, with a very high complexity of 1950 bits/cell, is the only phase in the list with complexity higher than horákite, phosphuranylite and kamitugaite (chemical complexity:

27–65 bits/fu, structural complexity: ~184 bits/cell). Consequently, hügelite is a very rare mineral in nature.

On the studied specimen, horákite and phosphuranylite occur in a close association; this may, in part, relate to their very similar structural complexities. We can only speculate that horákite formed contemporaneously with phosphuranylite.

Acknowledgements. We thank Pavel Škácha (Mining Museum Příbram, Czech Republic) for microphotography of horákite. The paper benefits from the thorough reviews of Travis Olds, František Veselovský and Frédéric Hatert. This research was supported by the project of GAČR No. 17-09161S to J.P. and J.S.

Electronic supplementary material. Supplementary crystallographic data for this paper are available online at the Journal web site (<http://dx.doi.org/10.3190/jgeosci.267>).

References

- ARDELEAN I, CORA S, IONCU V (2006) Structural investigation of $CuO-Bi_2O_3-B_2O_3$ glasses by FT-IR, Raman and UV-VIS spectroscopies. *J Optoelectron Adv Mater* 8: 18430–1847

- ASTILLEROS JM, PINTO AJ, GONÇALVES MA, SÁNCHEZ-PASTOR N, FERNÁNDEZ-DÍAZ L (2013) In situ nanoscale observations of metatorbernite surfaces interacted with aqueous solutions. *Environ Sci Technol* 47: 2636–2644
- BARTLETT JR, COONEY RP (1989) On the determination of uranium–oxygen bond lengths in dioxouranium(VI) compounds by Raman spectroscopy. *J Molecul Struct* 193: 295–300
- BLATOV VA, SHEVCHENKO AP, PROSERPIO DM (2014) Applied topological analysis of crystal structures with the program package ToposPro. *Cryst Growth Des* 14: 3576–3586
- BROWN ID (2002) *The Chemical Bond in Inorganic Chemistry. The Bond Valence Model*. Oxford University Press, Oxford, pp 1–278
- BUCK EC, BROWN NR, DIETZ NL (1995) Contaminant uranium phases and leaching at the Fernald Site in Ohio. *Environ Sci Technol* 30: 81–88
- BURNS PC, EWING RC, HAWTHORNE FC (1997) The crystal chemistry of hexavalent uranium: polyhedron geometries, bond-valence parameters, and polymerization of polyhedra. *Canad Mineral* 35: 1551–1570
- CANTRELL KJ, DEUTSCH WJ, LINDBERG MJ (2011) Thermodynamic model for uranium release from Hanford Site Tank residual waste. *Environ Sci Technol* 45: 1473–1480
- CATALANO JG, MCKINLEY JP, ZACHARA JM, HEALD SM, SMITH SC, BROWN GE (2006) Changes in uranium speciation through a depth sequence of contaminated Hanford sediments. *Environ Sci Technol* 40: 2517–2524
- ČEJKA J (1999) Infrared spectroscopy and thermal analysis of the uranyl minerals. In: BURNS PC, EWING RC (eds) *Uranium: Mineralogy, Geochemistry and the Environment*. Mineralogical Society of America and Geochemical Society Reviews in Mineralogy and Geochemistry 38: pp 521–622
- DAL BO F, HATERT F, BAIJOT M, PHILIPPO S (2015) Crystal structure of arsenuranoapatite from Rabejac, Lodève, France. *Eur J Mineral* 27: 589–597
- DEMARTIN F, DIELLA V, DONZELLI S, GRAMACIOLLI CM, PILATI T (1991) The importance of accurate crystal structure determination of uranium minerals. I. Phosphuranylite $\text{KCa}(\text{H}_3\text{O})_3(\text{UO}_2)_7(\text{PO}_4)_4\text{O}_4 \cdot 8\text{H}_2\text{O}$. *Acta Crystallogr B* 47: 439–466
- FINCH RJ, MURAKAMI T (1999) Systematics and paragenesis of uranium minerals. In: BURNS PC, FINCH RJ (eds) *Uranium: Mineralogy, Geochemistry and the Environment*. Mineralogical Society of America and Geochemical Society Reviews in Mineralogy 38: pp 91–180
- FROST RL, ČEJKA J, SEJKORA J, PLÁŠIL J, REDDY BL, KEEFFE EC (2011) Raman spectroscopic study of a hydroxy-arsenate mineral containing bismuth – atelestite, $\text{Bi}_2\text{O}(\text{OH})(\text{AsO}_4)$. *Spectrochim Acta, Part A*: 494–496
- GAGNÉ OC, HAWTHORNE FC (2015) Comprehensive derivation of bond-valence parameters for ion pairs involving oxygen. *Acta Crystallogr B* 71: 562–578
- GÖB S, GÜHRING J-E, BAU M, MARKL G (2013) Remobilization of U and REE and the formation of secondary minerals in oxidized U deposits. *Amer Miner* 98: 530–548
- GUNTER ME, BANDLI BR, BLOSS FD, EVANS SH, SU SC, WEAVER R (2004) Results from a McCrone spindle stage short course, a new version of EXCALIBUR, and how to build a spindle stage. *The Microscope* 52: 23–39
- HLOUŠEK J, PLÁŠIL J, SEJKORA J, ŠKÁCHA P (2014) News and new minerals from Jáchymov, Czech Republic (2003–2014). *Bull mineral-petrolog odd Nár Muz (Praha)* 22: 155–181 (in Czech with English abstract)
- ILTON ES, ZACHARA JM, MOORE DA, MCKINLEY JP, ECKBERG AD, CAHILL CL, FELMY AR (2010) Dissolution study of metatorbernite: thermodynamic properties and the effect of pH and phosphate. *Environ Sci Technol* 44: 7521–7526
- KRAUS W, NOLZE G (1996) POWDER CELL: a program for the representation and manipulation of crystal structures and calculation of the resulting X-ray powder patterns. *J appl Crystallogr* 29: 301–303
- KRIVOVICHEV SV (2009) Graph theory applied to low dimensional structural units in inorganic oxysalts. In: KRIVOVICHEV SV (ed) *Structural Crystallography of Inorganic Oxysalts*. IUCr Monographs on Crystallography 22. Oxford University Press, Oxford, pp 6–93
- KRIVOVICHEV SV (2010) Actinyl compounds with hexavalent elements (S, Cr, Se, Mo) – structural diversity, nanoscale chemistry, and cellular automata modeling. *Eur J Inorg Chem* 18: 2594–2603
- KRIVOVICHEV SV (2012) Topological complexity of crystal structures: quantitative approach. *Acta Crystallogr A* 68: 393–398
- KRIVOVICHEV SV (2013) Structural complexity of minerals: information storage and processing in the mineral world. *Mineral Mag* 77: 275–326
- KRIVOVICHEV SV (2014) Which inorganic structures are the most complex? *Angew Chem Int Ed Engl* 53: 654–661
- KRIVOVICHEV SV (2016) Structural complexity and configurational entropy of crystals. *Acta Crystallogr B* 72: 274–276
- KRIVOVICHEV SV (2017) Hydrogen bonding and structural complexity of the $\text{Cu}_3(\text{AsO}_4)(\text{OH})_3$ polymorphs (clinoclase, gilmarite): a theoretical study. *J Geosci* 62: 79–85
- KRIVOVICHEV SV, PLÁŠIL J (2013) Mineralogy and crystallography of uranium. In: BURNS PC, SIGMON GE (eds) *Uranium: From Cradle to Grave*. Mineralogical Association of Canada Short Courses 43: pp 15–119
- LIBOWITZKY E (1999) Correlation of O–H stretching frequencies and O–H···O hydrogen bond lengths in minerals. *Monatsh Chem* 130: 1047–1059
- LOCOCK AJ (2007) Trends in actinide compounds with the autunite sheet–anion topology. *Zap Vser Mineral Obshchest* 136: 115–137

- LOCOCK AJ, BURNS PC (2003) The structure of hügelite, an arsenate of the phosphuranylite group, and its relationship to dumontite. *Mineral Mag* 67: 1109–1120
- LOCOCK AJ, BURNS PC, FLYNN TM (2005) The role of water in the structures of synthetic hallimondite, $Pb_2[(UO_2)(AsO_4)_2](H_2O)_n$ and synthetic parsonsite, $Pb_2[(UO_2)(PO_4)_2](H_2O)_n$, $0 \leq n \leq 0.5$. *Amer Miner* 90: 240–246
- LUSSIER AJ, LOPEZ RAK, BURNS PC (2016) A revised and expanded structure hierarchy of natural and synthetic hexavalent uranium compounds. *Canad Mineral* 54: 177–283
- MAHER K, BARGAR JR, BROWN GE, JR (2013) Environmental speciation of actinides. *Inorg Chem* 52: 3510–3532
- MANDARINO JA (1976) The Gladstone-Dale relationship – Part I: derivation of new constants. *Canad Mineral* 14: 498–502
- MEREITER K (1982) The crystal structure of walpurgite, $(UO_2)Bi_4O_4(AsO_4)_2 \cdot 2H_2O$. *Tschermaks Mineral Petrogr Mitt* 30: 129–139
- NAKAMOTO K (1986) Infrared and Raman Spectra of Inorganic and Coordination Compounds. J. Wiley and Sons, New York, pp 1–496
- OK KM, BAEK J, HALASYAMANI PS, O'HARE D (2006) New layered uranium phosphate fluorides: syntheses, structures, characterizations, and ion-exchange properties of $A(UO_2)F(HPO_4) \cdot xH_2O$ ($A = Cs^+, Rb^+, K^+$; $x = 0-1$). *Inorg Chem* 45: 10207–10214
- ONDRUŠ P, VESELOVSKÝ F, GABAŠOVÁ A, HLOUŠEK J, ŠREIN V, VAVŘÍN I, SKÁLA R, SEJKORA J, DRÁBEK M (2003) Primary minerals of the Jáchymov ore district. *J Czech Geol Soc* 48: 19–147
- PETŘÍČEK V, DUŠEK M, PALATINUS L (2014) Crystallographic computing system JANA2006: general features. *Z Kristallogr* 229: 345–352
- PIRET P, PIRET-MEUNIER J (1988) Nouvelle détermination de la structure cristalline de la dumontite $Pb_2[(UO_2)_3O_2(PO_4)_2] \cdot 5H_2O$. *Bull Minéral* 111: 439–442
- PLÁŠIL J (2014) Oxidation–hydration weathering of uraninite: the current state-of-knowledge. *J Geosci* 59: 99–114
- PLÁŠIL J (2017) A novel sheet topology in the structure of kamitugaite, $PbAl[(UO_2)_5(PO_4)_{2.38}(AsO_4)_{0.62}O_2(OH)_2](H_2O)_{11.5}$. *J Geosci* 62: 253–260
- PLÁŠIL J (2018) Uranyl-oxide hydroxy–hydrate minerals: their structural complexity and evolution trends. *Eur J Mineral* 30: 237–251
- PLÁŠIL J, SEJKORA J, ONDRUŠ P, VESELOVSKÝ F, BERAN P, GOLIÁŠ V (2006) Supergene minerals in the Horní Slavkov uranium ore district, Czech Republic. *J Czech Geol Soc* 51: 149–158
- PLÁŠIL J, SEJKORA J, ČEJKA J, ŠKODA R, GOLIÁŠ V (2009) Supergene mineralization of the Medvědin uranium deposit, Krkonoše Mountains, Czech Republic. *J Geosci* 54: 15–56
- PLÁŠIL J, ŠKÁCHA P, SEJKORA J, ŠKODA R, NOVÁK M, VESELOVSKÝ F, HLOUŠEK J (2017) Babánekite, $Cu_3(AsO_4)_2 \cdot 8H_2O$, from Jáchymov, Czech Republic – a new member of the vivianite group. *J Geosci* 62: 261–270
- POUCHOU JL, PICOIR F (1985) “PAP” (φρΖ) procedure for improved quantitative microanalysis. In: ARMSTRONG JT (ed) *Microbeam Analysis*. San Francisco Press, San Francisco, pp 104–106
- ROH Y, LEE SR, CHOI S-K, ELLESS MP, LEE SY (2000) Physicochemical and mineralogical characterization of uranium-contaminated soils. *Soil Sediment Contam* 9: 463–486
- SEJKORA J, ČEJKA J, HLOUŠEK J, ŠREIN V, NOVOTNÁ M (2002) Phosphatian walpurgite from Smrkovec, the Slavkovský Les Mts. (the Czech Republic): its description and physico-chemical characteristics. *Neu Jb Mineral, Mh* 8: 353–367
- SEJKORA J, ČEJKA J, HLOUŠEK J, NOVÁK M, ŠREIN V (2004) Phosphowalpurgite, the (PO_4) -dominant analogue of walpurgite, from Smrkovec, Slavkovsky Les Mountains, Czech Republic. *Canad Mineral* 42: 963–972
- SEJKORA J, ČEJKA J, KOLITSCH U (2008) Uranosphaerite from Horní Halže near Měděnec (Krušné hory Mountains, Czech Republic): description and vibrational characteristics. *Neu Jb Mineral, Abh* 185: 91–98
- SEREZHKINA LB, TRUNOV VK, KHOLODKOVSKAYA LN, KUCHUMOVA, NV (1990) Crystalline-structure of $KUO_2CrO_4(OH) \cdot 1.5H_2O$. *Koordinats Khim* 16: 1288–1291
- SEREZHKINA LB, PERESYPKINA EV, VIROVETS AV, PUSHKIN DV, VEREVKIN AG (2010) Synthesis and structure of $Cs[UO_2(SeO_4)(OH)] \cdot nH_2O$ ($n = 1.5$ or 1). *Kristallografija* 55: 416–420
- SHANNON RD (1976) Revised effective ionic radii and systematic studies of interatomic distances in halides and chalcogenides. *Acta Cryst A* 32: 751–767
- SHELDRIK GM (2015) SHELXT – integrated space-group and crystal-structure determination. *Acta Crystallogr A* 71: 3–8
- SHIDRA O, ZENKO DS, KRIVOVICHEV SV (2014) Structural complexity of lead silicates: crystal structure of $Pb_{21}[Si_7O_{22}]_2[Si_4O_{13}]$ and its comparison to hyttsjöite. *Amer Miner* 99: 817–823